Facet Engineering of Pd Nanocrystals for Enhancing Photocatalytic Hydrogenation: Modulation of Schottky Barrier Height and Enrichment of Surface Reactants

Suwei Lu,[a] Bo Weng,[b]* Aizhu Chen,[a] Xinwei Li,[a] Haowei Huang,[b] Xiaoming Sun,[c]* Wenhui Feng,[d] Yanhua Lei,[e] Qingrong Qian,[a] and Min-Quan Yang[a]*

[a] College of Environmental Science and Engineering, Fujian Key Laboratory of Pollution Control & Resource Reuse, Engineering Research Center of Polymer Green Recycling of Ministry of Education, Fujian Normal University, Fuzhou 350007, P. R. China

[b] cMACS, Department of Microbial and Molecular Systems, KU Leuven, Celestijnenlaan 200F, 3001 Leuven, Belgium

[c] School of Materials Science and Engineering, National Institute for Advanced Materials, Nankai University, Tianjin 300350, P. R. China

[d] Hunan Province Key Laboratory of Applied Environmental Photocatalysis, Changsha University, Changsha 410022, P. R. China

[e] Hunan Provincial Key Laboratory of Xiangnan Rare-Precious Metals Compounds and Application, Department of Chemistry and Life Science, Xiangnan University, Chenzhou, 423000, P. R. China

**To whom correspondence should be addressed*

E-mail: bo.weng@kuleuven.be; xmsun@nankai.edu.cn; yangmq@fjnu.edu.cn

Abstract

Metal co-catalyst loading is one of the most widely explored strategy in promoting photocatalytic solar energy conversion. Engineering surface active facets of metal cocatalyst and exploring how they modulate the reactivity is crucial for the further development of advanced photocatalysts. In this work, through controlled hybridization of two-dimensional (2D) TiO_2 nanosheets with well-designed Pd nanocube (Pd NC) with exposed {100} facet and Pd nanooctahedron (NO) with exposed {111} facet, we unravel the distinct crystal facet effect of Pd cocatalyst in promoting the selective hydrogenation of nitroarenes to amines of TiO_2 photocatalyst. The activity tests show that the Pd NO with {111} facet is a more efficient cocatalyst than the Pd NC with exposed {100} facet. The prepared TiO_2-Pd NO composite displays a 900% enhancement of photocatalytic hydrogenation rate in comparison with bare TiO_2, while the TiO_2-Pd NC sample only shows a 200% photoactivity enhancement. Microscopic mechanism study discloses that the distinctive photoactivity improvement of Pd NO is ascribed to the concurrent modulation of Schottky barrier height and enrichment of surface reactants: (i) the Pd NO with lower fermi level could result in steeper band bending of TiO_2 (*i.e.*, higher Schottky barrier) than Pd NC, which is more efficient in boosting interfacial separation and inhibiting the recombination of photoexcited charge pairs; (ii) the {111} facet of Pd has higher nitroarenes adsorption ability and especially stronger hydrogen enrichment capability, thus accelerating surface hydrogenation process and contributing to higher reaction rate. This work emphasizes the rational facet control of cocatalyst for enhancing the photocatalytic hydrogenation performance.

Keywords: Surface crystal facet; Palladium cocatalyst; Schottky barrier; Surface reactant enrichment; Photocatalysis; Selective hydrogenation

Introduction

Catalytic hydrogenation represents a class of fundamental yet significant organic transformation in chemical industry.[1-3] It involves the addition of hydrogen to a large group of unsaturated organics with double or triple bonds, such as aldehydes, alkenes, alkynes, aromatic nitro-compounds and other derivatives with the assistance of catalysts, which are critical for fine chemicals, agrochemicals and pharmaceuticals production.[2, 4] Traditionally, the catalytic hydrogenation is carried out in the presence of stoichiometric metals (*e.g.*, Fe, Zn, Sn, and Al), and hydride reagents such as sodium borohydride, ammonia borane or molecular hydrogen (H_2).[5] In spite of the effectiveness, these conventional hydrogenation processes suffer from some inherent limitations of harsh reaction conditions (*e.g.*, high pressure and temperature), generation of undesirable side products, or high cost.[6]

Alternatively, photocatalytic hydrogenation has aroused continuous research interest due to its unique advantages of using solar energy and operating under mild conditions.[3, 7] Hydrogen species can be in-situ photogenerated on the catalyst surface without adding a reducing agent, thus offering a fascinating alternative strategy.[8] However, the photocatalytic hydrogenation typically faces problem of low catalytic efficiency on account of the severe charge carriers recombination and short of surface reactive sites.[9-11] Therefore, the artful design of advanced photocatalysts to facilitate charge separation and promote surface redox reaction is an enduring theme.[12, 13] As an significant metal oxide semiconductor, titanium dioxide (TiO_2) is extensively studied in photocatalysis due to its well stability and high reactivity. In recent years, anatase TiO_2 nanosheets containing large exposure of {001} facet attracts widespread attention owing to the observation that the {001} facet with a high surface energy is effective for dissociative adsorption of the reactant molecules.[14,15] Nevertheless, the performance of single-component semiconductor photocatalyst is still limited. To solve this problem, metal cocatalyst loading is one of the research hotspots due to its versatility for improving photocatalytic performance of different types of photoactive substrates.[16-19] It is well-recognized that the incorporation of metal cocatalyst with photoactive substrate could greatly facilitate charge separation by taking advantage of the Schottky junction, and the acceleration of surface redox reactions by serving as highly active sites, thereby significantly enhancing the photocatalytic efficiency. [20, 21]

Among the various metal cocatalysts, palladium (Pd) occupies a prominent place because of its compatibility with multiple functionalities.[22-26] In particular, metal Pd is a special material that has a strong affinity for hydrogen. It displays a number of exceptional properties in interaction with hydrogen, including (i) superior dissociation ability of hydrogen with little or no activation energy barrier; (ii) high adsorption and storage of hydrogen under ambient temperature and pressure, and (iii) accessible desorption of hydrogen.[27] These features enable the Pd to be an excellent candidate for catalyzing hydrogenation reactions.[28] However, the Pd metal in hybrid systems is generally in irregular sphere shape with mixed crystal facets. Owing to that the exposed facet of metal influences the interfacial contact with photoactive substrate for charge transfer and determines the arrangement of surface atoms acting as main active sites, the irregular, poorly defined Pd shapes with multiple types of surface atomic structures inherently hinder the optimization of the interfacial charge separation and limit the exposure of active sites on all the surfaces.[29, 30] As a result, the utilization efficiency of Pd nanoparticles and the photoactivity of the fabricated hybrid catalysts is restricted. Moreover, the inhomogeneously mixed facets of Pd also make it hard to identify the active surface structure and investigate the structure-activity characteristics, thus hampering the understanding of the intrinsic catalytic mechanism.[29] Recently, research works show that rational crystal surface engineering of cocatalysts is effective to tackle these problems.[31] The crystal surface engineering of Pd nanoparticles has demonstrated to modulate the photocatalytic performance toward solar fuel generation.[31,32] However, the influence of Pd crystal facet on the hydrogenation reaction is still unclear. In this context, to maximize the promoting effect of Pd cocatalyst for designing more efficient Pd-based photocatalytic systems toward hydrogenation reaction, it is highly desirable to control the crystal facet and investigate the shape effects of Pd cocatalysts.

Here, we report the specific active facets of Pd cocatalyst for enhancing photocatalytic hydrogenation by engineering different exposed surface facets of Pd. Well-defined Pd nanocube (NC) with exposed {100} facet and Pd nanooctahedron (NO) with exposed {111} facet are synthesized and assembled onto two-dimensional (2D) TiO_2 nanosheets to elucidate the significant surface facet effect. The photocatalytic performances of the fabricated TiO_2-Pd composites are evaluated by selective hydrogenation of aromatic nitro organics to amines, which is one of the most fundamental transformations widely involved in industrial fine chemicals production. The optimized TiO_2-Pd NO composite shows a remarkable photoactivity enhancement in comparison with bare TiO_2 (900 % enhancement), while the TiO_2-Pd NC sample only shows a 200% photoactivity enhancement. Characterizations reveal that the Pd NO not only more efficiently facilitates interfacial charge carrier transfer than Pd NC caused by its lower fermi level, but also enriches more reactant molecules on the catalyst surface to accelerate hydrogenation process due to its stronger hydrogen adsorption capability, thus synergistically leading to the better photocatalytic performance of the TiO_2-Pd NO composites.

Results and discussion

In the work, two-dimensional (2D) TiO_2 nanosheets are firstly prepared by a hydrothermal method (**Figure S1**, Supporting Information). It is employed as semiconductor substrate to hybrid with Pd due to its well stability and high reactivity. The nanosheet structure of the TiO_2 with large flat surface provides a good platform to support Pd component, while the thin thickness decreases the charge diffusion length and reduces their recombination probability, which are beneficial for the fabrication of advanced TiO_2-Pd hybrid photocatalyst. The Pd nanocube (NC) and Pd nanooctahedron (NO) are successfully synthesized by adjusting the different exposed surface facets, as shown in **Figure S2**. Then, Pd NC and Pd NO are assembled onto the surface of TiO_2 nanosheets by a wet impregnation method, as illustrated in **Figure 1a**. The detailed morphology and composition characterization of the samples have been carried out by transmission electron microscopy (TEM) analysis, as presented in **Figure 1b** and **c**. The high resolution TEM images of the TiO_2-Pd NC reveal that the lattice fringes of Pd NC are 0.195 nm (**Figure 1b**), corresponding to the {200} facets of Pd.[17,33] In comparison, the Pd NO shows lattice spacing of 0.225 nm, which can be attributed to the {111} facet of Pd (**Figure 1c**).[34,35] The analysis indicates that the Pd cube and octahedron are single crystals surrounded by six {100} facets or eight {111} facets, respectively.

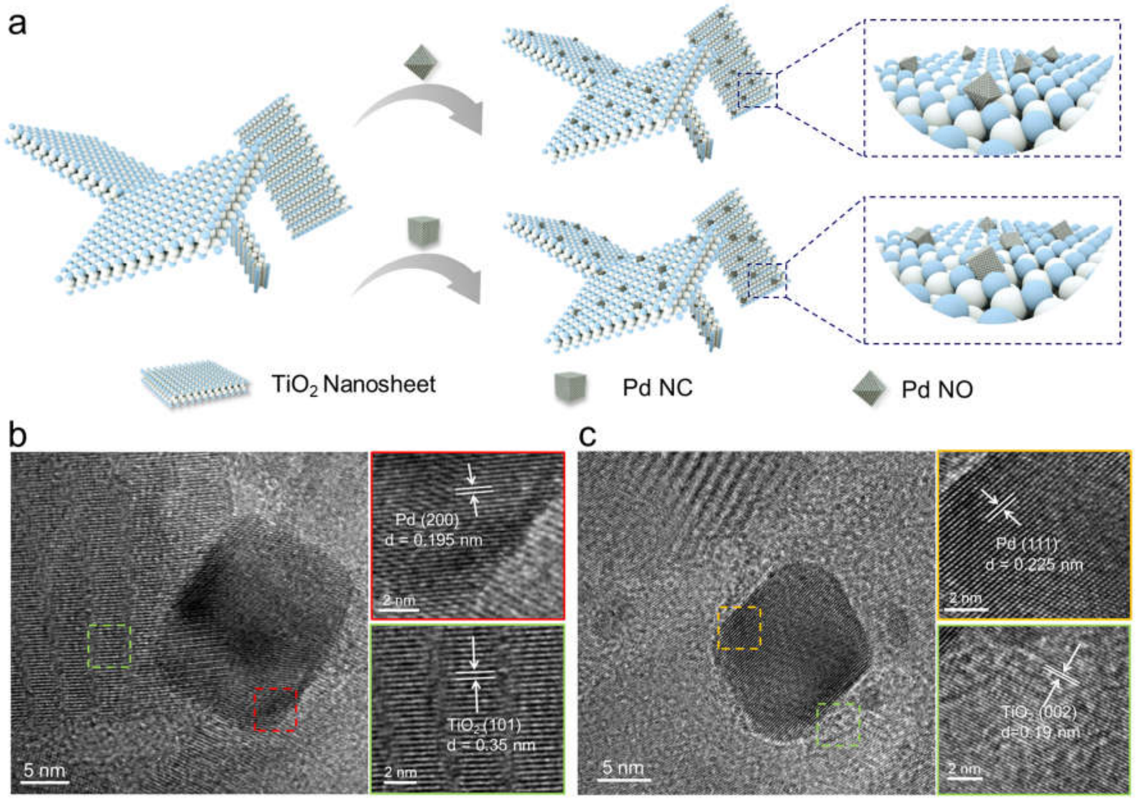

Figure 1. Schematic synthesis of TiO_2-Pd NC and TiO_2-Pd NO composites (a); high-resolution TEM images of TiO_2-Pd NC (b) and TiO_2-Pd NO (c) samples.

Figure 2a and **Figure S3** show the crystal structures of the bare TiO_2, TiO_2-Pd NC and TiO_2-Pd NO composites, which are characterized by powder x-ray diffraction (XRD). All the samples exhibit similar XRD patterns. The identified peaks are well consistent with anatase TiO_2 (JCPDS No. 21-1272). When the addition amount of Pd nanocrystals reaches 2%, metallic Pd diffraction peaks are observed over both the TiO_2-2Pd NC and TiO_2-2Pd NO composites (**Figure S3**), confirming the formation of hybrid composite. In addition, Raman spectroscopy is further used to analyze the phase composition of the fabricated photocatalysts. The Raman analysis is sensitive to the microstructure and crystallinity of materials, thus can provide detailed information about chemical structure and molecular interactions. As illustrated in **Figure 2b**, five vibration peaks are observed at 144 (Eg), 199 (Eg), 394 (B1g), 514 (A1g), and 636 cm^{-1} (Eg), which belong to the anatase TiO_2 vibration mode.[36-38] The result verifies that anatase TiO_2 are the primary species, in conformity with the XRD analysis. Notably, after the decoration of Pd NC and Pd NO, the Raman peak located at 146 cm^{-1} in TiO_2-0.5Pd NC and TiO_2-0.5Pd NO composites shifts toward high wavenumber as compared to that of bare TiO_2, suggesting that the symmetric stretching vibration of O−Ti−O in TiO_2 is affected.[36, 39] This can be ascribed the strong chemical interaction between the oxygen in TiO_2 and metal Pd.[40] The accurate amount of Pd nanoparticles in the TiO_2-Pd composites have been evaluated by the inductively coupled plasma-optical emission spectrometry (ICP-OES). As presented in in **Table S1**, the addition amounts of Pd NC and Pd NO in the TiO_2-0.5Pd NC and TiO_2-0.5Pd NO composites are measured to be 0.473% and 0.486%, respectively, which is approximate to the theoretical amount (*i.e.*, 0.5%).

The impact of metal Pd loading on the structure of TiO_2 has been further revealed by X-ray photoelectron spectra (XPS) analysis through studying the surface valence states of the elements in the TiO_2, TiO_2-0.5Pd NC and TiO_2-0.5Pd NO composites. **Figure 2c** shows that the Ti 2p spectrum of TiO_2 exhibits two peaks at 458.4 and 464.1 eV assigned to Ti $2p_{3/2}$ and Ti $2p_{1/2}$, respectively.[41, 42] After loading Pd nanocrystals (*i.e.*, Pd NC and NO), slight shift of Ti 2p peaks toward higher binding energy over the TiO_2-0.5Pd NC and TiO_2-0.5Pd NO composites are observed. Correspondingly, the binding energies for O 1s spectrum in TiO_2-0.5Pd NC and TiO_2-0.5Pd NO composites are higher than that of TiO_2 (**Figure 2d**). Moreover, in comparison with the binding energies of metallic Pd (335.4 eV for Pd $3d_{5/2}$ and 340.6 eV for Pd $3d_{3/2}$),[43] the Pd 3d peaks of the TiO_2-0.5Pd NC and TiO_2-0.5Pd NO are negatively changed (**Figure 2e**). The obvious XPS shifts are resulted from the alterations of coordinated environment or chemical state of the elements in hybrid composites, in which the Pd atoms with empty d orbitals could accept lone pair electrons of oxygen in TiO_2.[17] The results further confirm the incorporation of metallic Pd into TiO_2, and the formation of chemical interaction between the Pd crystals and the TiO_2.

Moreover, UV-vis diffuse reflectance spectra (DRS) have been employed to investigate the optical properties of the bare TiO_2 and TiO_2-Pd composites. As illustrated in **Figure 2f** and **Figure S4** (Supporting Information), all of the samples exhibit analogous light absorption fingerprints with band edges of around 400 nm, corresponding to the inherent band gap absorption of anatase TiO_2.[44] After the addition of small amount of metallic Pd, both the TiO_2-Pd NC and TiO_2-Pd NO composites display improved visible light absorption as compared to TiO_2, which is originated from the essential light absorption of the Pd nanocrystals (NC and NO) and the light scattering caused by the Pd nanocrystals.[17,49,50] Specifically, (i) although Pd is nonplasmonic metal, it is still able to capture solar light due to inter-band transition of bound electrons (in filled energy bands lower than the conduction band), thus resulting in visible light absorption of the TiO_2-Pd; (ii) after the integration of Pd with TiO_2, the Pd metal nanocrystals are much more closely packed on the TiO_2 support, which could lead to high scattering of light at longer wavelengths.[49, 50] Consequently, the two factors contribute to the high visible light absorption of the TiO_2-Pd composites as compared with bare TiO_2. [17,45,46] Additionally, the optical property of TiO_2-Pd NC composites is similar with that of TiO_2-Pd NO samples in both ultraviolet and visible regions, demonstrating that the morphology of metallic Pd has no remarkable impact on the light absorption properties of the TiO_2-Pd NC and TiO_2-Pd NO composites.

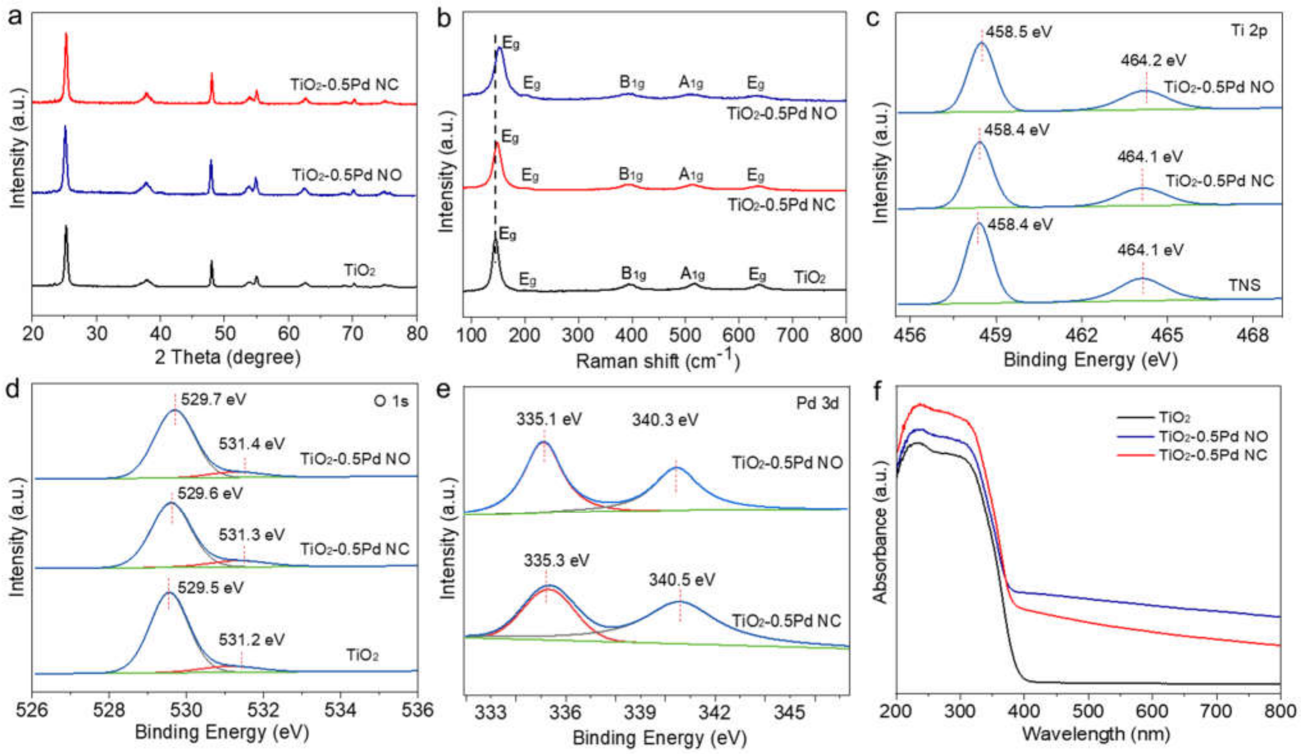

Figure 2. XRD patterns (a), Raman spectra (b), high-resolution XPS spectra of Ti 2p (c), O 1s (d), Pd 3d (e) core levels, and DRS spectra (f) of TiO_2, TiO_2-0.5Pd NC and TiO_2-0.5Pd NO composites.

In the following, the photocatalytic activity of TiO_2, TiO_2-Pd NC and TiO_2-Pd NO composites have been tested by selective hydrogenation of aromatic nitro-compounds to amines in aqueous phase. Ethanol is used as quencher to trap photogenerated holes. Photocatalytic hydrogenation of 4-nitroaniline (4-NA) to corresponding 4-phenylenediamine (4-PDA) is firstly performed. It is a typical six-electron hydrogenation reaction (**Figure S5**). **Figure S6** shows that upon light irradiation, the peak corresponding to 4-NA at 382 nm gradually decreases, while a new absorption peak belonging to 4-

PDA at 300 nm is concomitantly generated.[47] Simultaneously, the solution at different reaction time has been collected and analyzed by gas chromatography (GC), which reveals that the reactant of 4-NA is transformed into 4-PDA through the photocatalytic hydrogenation without other by-products (**Figure S7**), approaching 100% selectivity. The photocatalytic activities of TiO_2-Pd NO with different Pd NO weight ratios are shown in **Figure 3a**. The addition of Pd nanocrystals plays a critical role on the photoactivity enhancement. Small amount of Pd (*e.g.*, 0.25%) noticeably improves the photocatalytic hydrogenation efficiency of TiO_2. By increasing the addition amount of Pd NO to 0.5%, the TiO_2-0.5Pd NO sample achieves the optimal synergistic interaction between TiO_2 and Pd NO, exhibiting the highest photoactivity. The conversion of 4-NA over the TiO_2-0.5Pd NO composite is nearly 100% within 16 min, about 9 times higher (900% enhancement) than that of TiO_2. In contrast, the photoactivity improvement is remarkably different for the TiO_2-Pd NC composites. As shown in **Figure 3b**, the TiO_2-0.25Pd NC composite exhibits a similar photoactivity as compared to blank TiO_2. In addition, although the TiO_2-0.5Pd NC sample with 0.5% Pd NC also displays the best photocatalytic activity, the photoactivity enhancement is less significant. The conversion of 4-NA over TiO_2-0.5Pd NC is about 30%, which is only 2-fold (200% enhancement) higher than that of blank TiO_2. The result indicates that the Pd NO and Pd NC are significantly different in promoting the photocatalytic hydrogenation performance of TiO_2.

Moreover, it is notable that the photocatalytic efficiencies of the TiO_2-Pd NO and TiO_2-Pd NC with 1% and 2% Pd are obviously decreased, suggesting the negative effect of the high Pd contents on the performance of the composites. The deterioration can be explained by the following two reasons. Firstly, the high weight content of Pd may prevent the light absorption of TiO_2 by scattering of photons and reduce the light intensity through the inside of the reaction solution.[48] Secondly, the Pd nanocrystals may serve as electron-hole recombination centers if the dosage levels exceed the optimum loading,[49] thus inhibiting the photocatalytic performance. The phenomenon is widely observed in Pd-based composite photocatalysts, which determines that in most cases, the addition amount of Pd is lower than 1% for achieving an optimal synergistic interaction with semiconductor.[13, 50] Furthermore, recent researches have shown that halides (i.e., Br^-) used in the synthesis of Pd crystal could be adsorbed on its surface, consequently decreasing the catalytic performance.[51] However, in this work, a two-step method with adequate washing is used to synthesize the TiO_2-Pd composites, which greatly reduces the amounts of residue halides on the catalyst surface of Pd crystal, as verified by the XPS analysis in **Figure S8**. Thus, the impact of halides on photocatalytic hydrogenation performance of the TiO_2-Pd composites is negligible.

To demonstrate the generically higher promotion effect of Pd NO than Pd NC, photocatalytic selective hydrogenation of other aromatic nitro-compounds, including 4-Nitroanisole; 1-Bromo-4-Nitrobenzene and 1-Chloro-4-Nitrobenzene over the bare TiO_2, TiO_2-0.5Pd NO and TiO_2-0.5Pd NC composites has been investigated. As shown in **Figure 3c**, the hybridization of metal Pd expectedly enhances the photoactivity of TiO_2 toward different nitro organics. Also, the TiO_2-0.5Pd NO sample exhibits better photocatalytic performance than the TiO_2-0.5Pd NC composite. Meanwhile, a comparison of the photocatalytic performance over different photocatalysts has been summarized, as listed in **Table S2**, revealing the advanced performance of the TiO_2-Pd NO photocatalyst. Finally, continuous photocatalytic hydrogenation experiment over the optimal TiO_2-Pd NO has been carried out to assess the stability of the composite. **Figure 3d** shows that no apparent performance degradation is detected during the five successive recycle tests for hydrogenation of 4-NA, suggesting the high photostability of the TiO_2-0.5Pd NO under the present reaction conditions. Meanwhile, the ICP-OES measurement suggests that the content of Pd in the solution after the reaction is neglectable, which further proves the stability of TiO_2-0.5Pd NO photocatalyst.

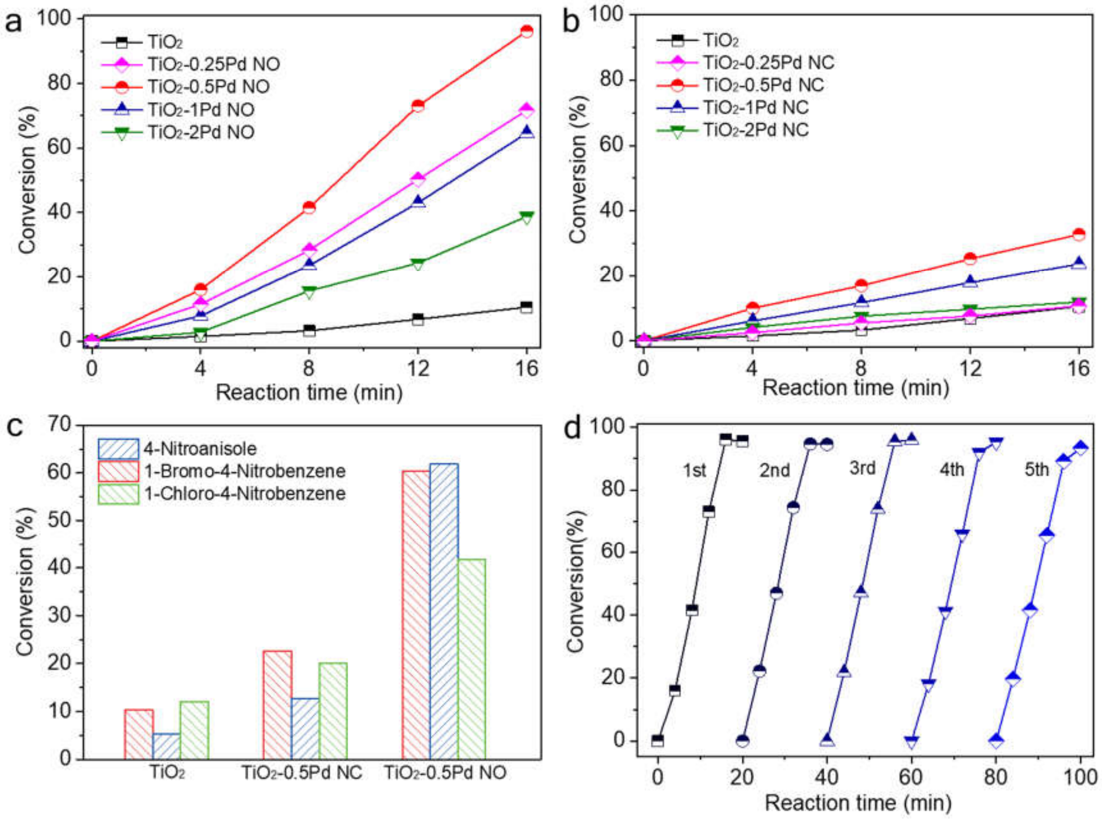

Figure 3. Photocatalytic hydrogenation of 4-NA to 4-PDA over blank TiO_2, TiO_2-Pd NO and TiO_2-Pd NC samples with different weight ratios of Pd (b); photocatalytic hydrogenation of 4-Nitroanisole; 1-bromo-4-nitrobenzene and 1-chloro-4-nitrobenzene over the TiO_2, TiO_2-0.5Pd NO and TiO_2-0.5Pd NC composites after 8 min reaction (c); recycling photocatalytic hydrogenation of 4-NA over TiO_2-0.5Pd NO sample (d). Reaction conditions: 30 mg sample in 40 mL aromatic nitro compounds solution (10 mg L^{-1}) with 100 µL ethanol, UV light ($\lambda = 365 \pm 15$ nm), N_2 atmosphere, reaction temperature, 298 K.

In short, the above photoactivity tests faithfully validate that the Pd NO cocatalyst is more efficient than the Pd NC for enhancing the photocatalytic hydrogenation activity. Given the same TiO_2 semiconductor substrate and the same method used for the fabrication of the TiO_2-Pd NO and the TiO_2-Pd NC composites, the marked photoactivity difference between the two series of catalysts can be ascribed to the different exposed facet of Pd in the hybrid composite. To reveal the underlying mechanism, collective theoretical and experimental analyses of bare TiO_2, TiO_2-Pd NO and TiO_2-Pd NC composites have been carried out.

Generally, the contact of metal with semiconductor forms Schottky barrier due to their different

Fermi levels (E_f). Electrons or holes (depending on the n-type or p-type semiconductor) will continuously transfer from semiconductor to metal until the E_f of the metal and the semiconductor reaches equilibrium. After the E_f alignment, a space-charge region forms on the semiconductor surface and results in band bending, as illustrated in **Figure S9** (supporting information). The bending (*i.e.*, the Schottky barrier height (Φ_B)) could inhibit the backflow of charge carriers from metal to semiconductor, which can be calculated from the following equation:

$\Phi_B = \Phi_M - X_{Semi}$ (1)

Φ_M is the working function of the metal, which is defined as the energy required for an electron transfer from the Fermi energy of the metal to vacuum. X_{Semi} is electron affinity, which is determined by the energy difference between the vacuum (V_{ac}) energy and the minimum conduction band (CB). For the TiO_2-Pd composites, including the TiO_2-Pd NO and the TiO_2-Pd NC, the E_f of the Pd is lower than that of the n-type TiO_2 semiconductor. Thus, electrons will flow from the TiO_2 nanosheets to the Pd nanocrystals, leading to the upward bend bending of TiO_2 toward the Pd surface after E_f equilibrium (**Figure 4a**). Notably, due to that the Φ_B is strongly affected by the Φ_M, while the surface state (surface atoms configuration) influences the Φ_M. Therefore, the different exposed facets of metal would result in different bend bending heights (Φ_B). As for the Pd NC with exposed {100} facet and Pd NO with exposed {111} facet, both the experimental studies and theoretical calculations have revealed that the Pd{111} surface possesses larger work function (lower E_f) than the Pd{100} surface.[52, 53] Specifically, the experimental work function values of Pd{111} and Pd{100} are 5.9 eV and 5.6 eV, respectively. As such, upon coupling with the TiO_2 nanosheets, the Pd NO with exposed {111}facet could cause steeper upward bending of the TiO_2 band and thus higher barrier heights than the Pd NC with {100} facet. This makes it harder for the backflow of electrons from Pd NO to TiO_2 semiconductor (**Figure 4a**). In this context, upon light irradiation, the formed TiO_2-Pd NO Schottky barrier will ensure the unidirectional transfer of photoexcited electrons across the TiO_2-Pd junction interface more efficiently. More electrons and holes can accumulate on the surfaces of Pd NO and TiO_2, respectively, thereby prolonging longer lifespan of photogenerated charges for reaction and leading to higher photoactivity of TiO_2. This has been experimentally testified by the following photoluminescence (PL) spectra and photo-electrochemical analyses.

As shown in **Figure 4b**, PL spectrum is used to investigate the recombination of photoexcited electron-hole pairs in the TiO_2, TiO_2-Pd NO and TiO_2-Pd NC composites.[54, 55] Similar PL curves are observed for the three samples, among which the blank TiO_2 exhibits the highest intensity. The diminished PL of TiO_2-0.5Pd NO and TiO_2-0.5Pd NC composites can be attributed to the fact that the decorated metal Pd nanocrystals act as "electron reservoirs" to trap the photoelectrons generated from TiO_2, thereby inhibiting the recombination of electron-hole pairs,[56] as depicted in **Figure S10**. Moreover, the PL intensity of TiO_2-0.5Pd NO composite is lower than the intensity of TiO_2-0.5Pd NC sample, indicating that the Pd NO is more efficient in inhibiting the charge carriers recombination. **Figure 4c** shows the transient photocurrent responses of the samples, which are recorded to study the transfer and separation of charge carriers. Generally, the higher photocurrent intensity, the more efficient transfer of charge carriers. It can be seen that both the TiO_2-0.5Pd NO and TiO_2-0.5Pd NC composites exhibit larger photocurrent value than blank TiO_2, indicating that the metal Pd has an accelerating effect on promoting the separation of charge carriers. The higher photocurrent intensity of the TiO_2-0.5Pd NO than that of the TiO_2-0.5Pd NC suggests the more sensitive transfer of photoelectrons from TiO_2 to Pd NO. Notably, the photocurrent intensity of TiO_2-0.5Pd NO sample gradually decreases under continuous light irradiation. The result can be attributed to the transfer of electrons in the CB of TiO_2 to the Pd NO, which accumulates and release gradually when the light is turned off, thus leading to a gradual decline of the photocurrent.[35]

Moreover, **Figure 4d** shows the polarization curves of the TiO_2 and TiO_2-Pd composites, which indicates that the introduction of metal Pd greatly improves the current density in the similar potential range due to the excellent electrons transfer efficiency of Pd. Additionally, Pd facet-dependent current density over TiO_2-Pd composites is observed. The Pd NO with {111} surface more efficiently increases the current density than the Pd NC with {100} surface due to the higher electronic conductivity of Pd NO.[35] **Figure 4e** displays the cyclic voltammograms (CV) curves of the bare TiO_2, TiO_2-0.5Pd NO and TiO_2-0.5Pd NC composites that are employed to elucidate the electron transfer rate of the samples.[57, 58] The obvious anodic and cathodic current density over these three samples follows the order of TiO_2-0.5Pd NO > TiO_2-0.5Pd NC > TiO_2, denoting the most effective transport of charge carriers from TiO_2 to Pd NO. The increased lifetime of photogenerated charge carriers is in consistent with the enhanced photoactivity of the TiO_2-0.5Pd NO composite as observed above.

Furthermore, the electrochemical impedance spectroscopy (EIS) Nyquist plots of bare TiO_2, TiO_2-

0.5Pd NO and TiO_2-0.5Pd NC composites have been measured to further understand the charge transfer at the contact interface between the electrode and electrolyte.[47, 59-62] As displayed in **Figure 4f**, all the three electrodes exhibit semicircles at high frequency. The Nyquist plots of TiO_2-0.5Pd NO and TiO_2-0.5Pd NC composites are depressed in comparison with that of TiO_2, while the TiO_2-0.5Pd NO displays the smallest arc radius. The result indicates the most efficient transfer of charge carriers over TiO_2-0.5Pd NO composite, demonstrating the crystal facet-dependent charge carrier transfer over metal Pd. In addition, compared with the bare TiO_2 and TiO_2-0.5Pd NC composite (**Figure 4g**), the corresponding Bode-phase plot of TiO_2-0.5Pd NO has been observed to shift to a lower frequency, which elucidates the retarded recombination and prolonged lifetime of electron-hole pairs.[63, 64] Collectively, the above characterizations clearly prove the critical facet effect of Pd cocatalyst on accelerating charges mobility and reducing the recombination possibility, thereby resulting in enhanced photocatalytic selective hydrogenation activity.

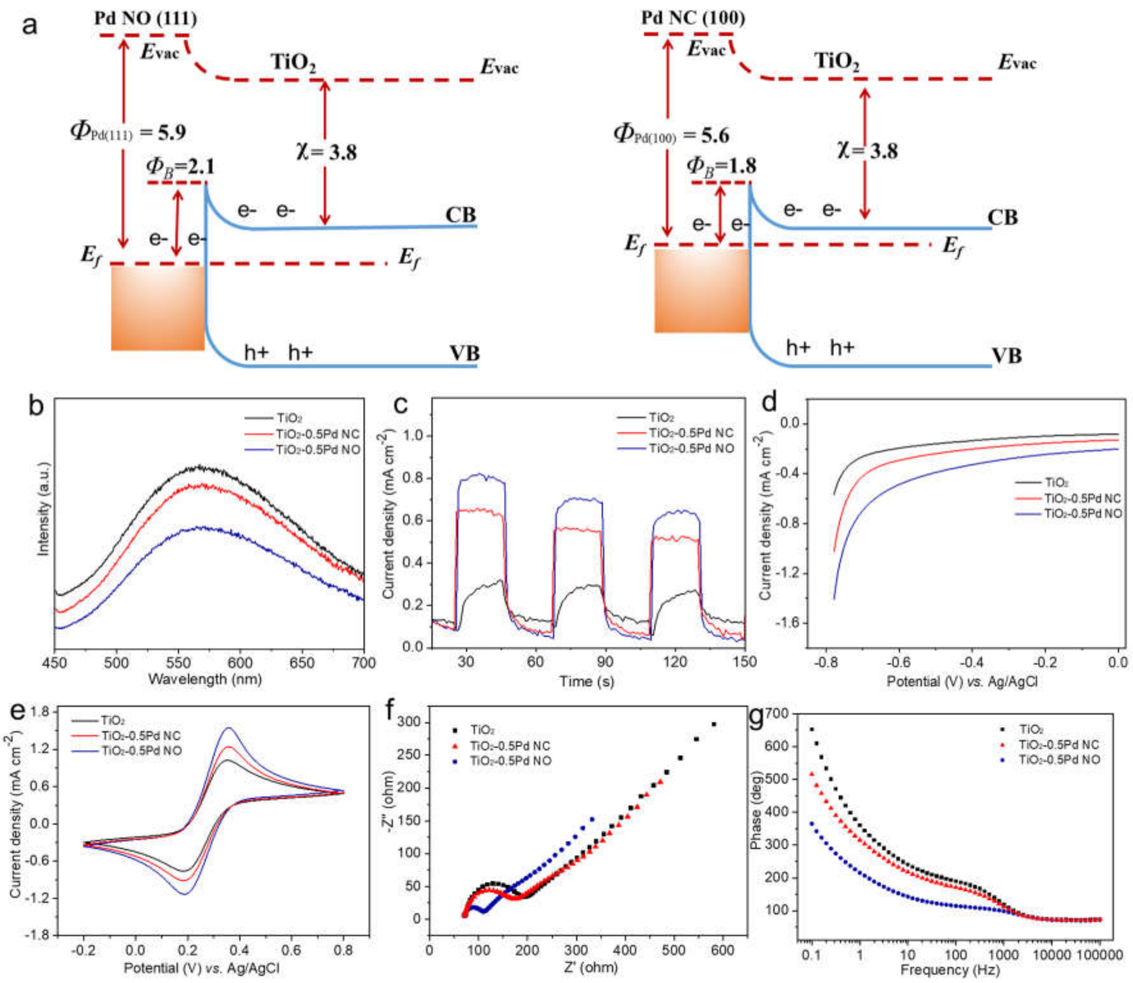

Figure 4. Schematic energy-band diagram of TiO_2-Pd NO and TiO_2-Pd NC composites (a); PL

emission spectra (b), transient photocurrent densities (c), polarization curves (d), cyclic voltammograms (e), EIS Nyquist plots (f), and corresponding Bode phase plots (g) of bare TiO_2, TiO_2-Pd NC and TiO_2-Pd NO composites.

Besides the separation of photoexcited electron-hole pairs, the surface reactant adsorption is another critical factor that determines the photocatalytic efficiency of catalysts due to that photocatalytic conversion is a heterogeneous catalytic process.[65, 66] Therefore, the surface area and porosity of the TiO_2, TiO_2-0.5Pd NO and TiO_2-0.5Pd NC samples have been investigated by nitrogen adsorption-desorption. As presented in **Figure S11** and **Table S3** (Supporting Information), the three samples process similar type IV adsorption-desorption isotherms with a typical H3 hysteresis loop.[67] The specific surface areas of TiO_2-0.5Pd NO and TiO_2-0.5Pd NC samples are comparable to the bare TiO_2, suggesting that the introduction of Pd nanocrystal has no remarkable effect on the surface area of these catalysts. However, the adsorption experiments in **Figure 5a** and **Figure S12** show the absorptivity enhancement for TiO_2-0.5Pd NO and TiO_2-0.5Pd NC composites due to the presence of metal Pd. This may be attributed to the interactions of π-complexation between the metal palladium and the aromatic reactants,[68, 69] which contributes to increasing the adsorption of reactants, *i.e.,* 4-NA.

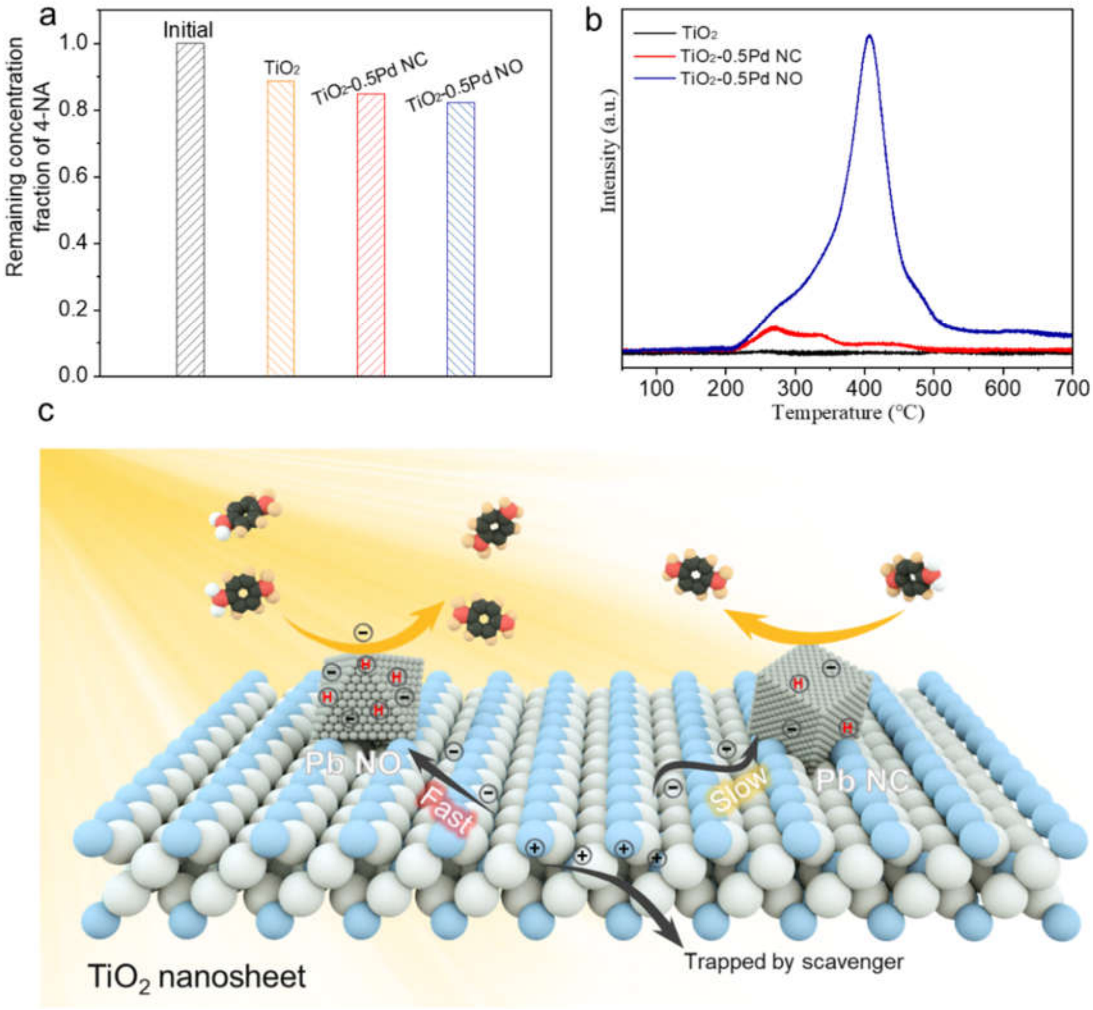

Figure 5. Column plots showing the remaining 4-nitroaniline in solution after being kept in dark for 1 h until adsorption equilibrium of the 4-nitroaniline solution over different samples (a); The temperature-programmed desorption (TPD) spectra of TiO_2, TiO_2-0.5Pd NO and TiO_2-0.5Pd NC composites (b); schematically illustrated reaction mechanism for photocatalytic hydrogenation of nitroarenes over TiO_2-Pd composites (c).

Moreover, since the photocatalytic hydrogenation of 4-NA involves the reaction with hydrogen species, the interaction of bare TiO_2, TiO_2-Pd NO and TiO_2-Pd NC with hydrogen has been tested by the temperature-programmed desorption (TPD) technique. As displayed in **Figure 5b**, for the bare TiO_2, no distinct desorption peaks are observed, indicating the poor adsorption of hydrogen. However, the TiO_2-0.5Pd NC composite shows two main broadened hydrogen desorption peaks located at *ca.* 268 °C and 336 °C, respectively, indicating the strong hydrogen adsorption affinity of Pd NC. Moreover, several stronger desorption peaks located at the range of 200-550 °C are detected for the

TiO_2-0.5Pd NO sample. Generally, the stronger the desorption peak, the higher the adsorption amount of hydrogen.[70] To theoretically analyze the difference of adsorption ability on hydrogen between TiO_2-0.5Pd NO and TiO_2-0.5Pd NC, the Vienna ab initio simulation package (VASP) has been used to analyze the Pd{100} and {111} facets based on the first-principles density functional theory (DFT). The free energy of atomic hydrogen adsorption (ΔG_H) is an important indicator for predicting the activity of hydrogenation reaction on the catalyst. In this case, the adsorption of H* (chemisorbed H atoms on the surface active sites of catalyst) is stronger when the value of ΔG_H is more negative. **Figure S13** shows the configurations of H adsorbate on the Pd{111} and Pd{100} surfaces, among which the corresponding adsorption energies are calculated as $\Delta G_{H\ Pd\{111\}}$ =-3.85 eV and $\Delta G_{H\ Pd\{100\}}$ = -3.81 eV, respectively. Obviously, the value of ΔG_H {111} is more negative than that of ΔG_H {100}, which suggests a stronger H* adsorption ability on the Pd NO with exposed {111} facet. The enhanced H* adsorption on the Pd NO surface as compared to that on Pd NC with exposed {100} surface is coordinated with the TPD analysis in **Figure 5b**, which is favorable for the photocatalytic hydrogenation reaction. Thus, the TiO_2-0.5Pd NO composite exhibits the strongest hydrogen adsorption capability among these three samples. This results in the enrichment of the hydrogen species on the surface of TiO_2-0.5Pd NO, which is favorable for the photocatalytic hydrogenation reaction. Therefore, the introduction of Pd NO onto TiO_2 not only accelerates the transfer of photoexcited charges, but also favors the surface enrichment of reactants, which thus concurrently promotes the catalytic efficiency toward selective hydrogenation of 4-NA.

Furthermore, controlled experiments have been carried out to explore the photocatalytic mechanism toward selective hydrogenation of nitro organics over the TiO_2-0.5Pd NO composite. As shown in **Figure S14**, when the hole scavenger, *i.e.*, ethanol, is removed from the reaction system, the photocatalytic hydrogenation efficiency of 4-NA decreases significantly, indicating the critical role of hole scavenger in improving the photoactivity. The presence of hole scavenger could retard the recombination of charge pairs and extend their lifetime, leading to photoactivity enhancement. Additionally, the effect of nitrogen on photocatalytic performance has also been investigated. Without nitrogen as inert atmosphere, the hydrogenation reaction is totally ceased in air under UV light irradiation, which is ascribed to the fact that the O_2 molecules in air are preferred to react with electrons to produce the superoxide radicals ($O_2^{\cdot -}$) due to the low redox potential (-0.046 V vs. RHE) as compared with that of 4-NA reduction (-0.3 V vs. RHE).[71-73] Based on the above experimental analyses and theoretical analyses, a tentative reaction mechanism for photocatalytic hydrogenation of organic compounds over TiO_2-0.5Pd NO composite has been proposed, as displayed in **Figure 5c**. Under light irradiation, electrons in the TiO_2 valence band (VB) are excited into the conduction band (CB), leaving holes in the VB. The electrons are localized from the TiO_2 to the deposited Pd nanocrystals, which inhibits their recombination with holes. Then, the adsorbed 4-nitroaniline molecules will hydrogenate in the presence of proton and photogenerated electrons to form 4-phenylenediamine. Notably, the hydrogen involved in the photocatalytic nitroaromatic hydrogenation is indeed from the water instead of the ethanol, as proven by Li and colleagues.[3] Concurrently, the holes in the VB of TiO_2 will be consumed by the hole scavenger of ethanol for inhibiting the electron-hole recombination, thus enhancing the photocatalytic activity. Since the Pd NO with exposed {111} surface exhibit the higher charge separation efficiency and stronger hydrogen enrichment capability than the Pd NC with exposed {100} surface, the TiO_2-Pd NO composite shows significant photoactivity enhancement as compared with TiO_2-Pd NC composite, demonstrating the facet effect of Pd nanocrystals toward photocatalytic selective hydrogenation.

Conclusion

In summary, Pd NC and NO with different exposed facets are introduced onto 2D TiO_2 to investigate the surface facets effect of Pd nanocrystals on the photocatalytic selective organic transformations. The photoactivities are evaluated by selective hydrogenation of aromatic nitro organics in aqueous media under UV light irradiation. The TiO_2-Pd NO composites reveal higher photocatalytic efficiency as compared with the TiO_2-Pd NC composites. Based on a series of theoretical and experimental analyses, the photoactivity improvement is due to the following two factors. On one hand, the Pd NO is more efficient in accelerating the separation and transportation of charge carriers than the Pd NC owing to its lower Fermi level. On the other hand, the hydrogenation process on the surface of Pd{111} facet is more preferable due to the strong proton enrichment capability, thus leading to the improved photocatalytic hydrogenation efficiency of 4-NA over TiO_2-Pd NO sample than that of TiO_2-Pd NC composite. This work clarifies the relationship between surface facets effect of Pd nanocrystals and photoactivity of Pd-semiconductor composites toward photocatalytic selective hydrogenation reaction.

Conflicts of interest

There are no conflicts to declare.

Acknowledgements

This work was financially supported by the National Natural Science Foundation of China (NSFC, 21905049, 21902132 and 21902133), the Award Program for Minjiang Scholar Professorship, the European Union's Horizon 2020 research and innovation programme under the Marie Skłodowska-Curie grant agreement No. 891276; Research Foundation-Flanders (FWO, grant No. 1280021N), and the Natural Science Foundation of Fujian Province (2020J01201). We would like to thank Prof. Dr. Jun Chen from Fujian Institute of Research on the Structure of Matter, Chinese Academy of Sciences, for discussions of theoretical calculations.

Supporting Information. The detailed preparation of catalyst samples and activity tests are described in the Supporting Information. Additional TEM images and characterization results. This material is available free of charge via the Internet at http://pubs.acs.org

References

(1) Smith, A. M.; Whyman, R.: Review of Methods for the Catalytic Hydrogenation of Carboxamides. *Chem. Rev.* **2014**, *114*, 5477-5510.

(2) Zang, W.; Li, G.; Wang, L.; Zhang, X.: Catalytic Hydrogenation by Noble-Metal Nanocrystals with Well-Defined Facets: A Review. *Catal. Sci. Technol.* **2015**, *5*, 2532-2553.

(3) Yu, Z.; Chen, Z.; Chen, Y.; Peng, Q.; Lin, R.; Wang, Y.; Shen, R.; Cao, X.; Zhuang, Z.; Li, Y.: Photocatalytic Hydrogenation of Nitroarenes Using $Cu_{1.94}S$-$Zn_{0.23}Cd_{0.77}S$ Heteronanorods. *Nano Res.* **2018**, *11*, 3730-3738.

(4) Bratlie, K. M.; Lee, H.; Komvopoulos, K.; Yang, P.; Somorjai, G. A.: Platinum Nanoparticle Shape Effects on Benzene Hydrogenation Selectivity. *Nano Lett.* **2007**, *7*, 3097-3101.

(5) Climent, M. J.; Corma, A.; Iborra, S.: Heterogeneous Catalysts for the One-Pot Synthesis of Chemicals and Fine Chemicals. *Chem. Rev.* **2011**, *111*, 1072-1133.

(6) Friedmann, D.; Hakki, A.; Kim, H.; Choi, W.; Bahnemann, D.: Heterogeneous Photocatalytic Organic Synthesis: State-of-the-Art and Future Perspectives. *Green Chem.* **2016**, *18*, 5391-5411.

(7) Yang, M.-Q.; Zhang, N.; Wang, Y.; Xu, Y.-J.: Metal-Free, Robust, and Regenerable 3D Graphene–Organics Aerogel with High and Stable Photosensitization Efficiency. *J. Catal.* **2017**, *346*, 21-29.

(8) Song, J.; Huang, Z.-F.; Pan, L.; Li, K.; Zhang, X.; Wang, L.; Zou, J.-J.: Review on Selective Hydrogenation of Nitroarene by Catalytic, Photocatalytic and Electrocatalytic Reactions. *Appl.*

Catal. B **2018**, *227*, 386-408.

(9) Hao, C. H.; Guo, X. N.; Pan, Y. T.; Chen, S.; Jiao, Z. F.; Yang, H.; Guo, X. Y.: Visible-Light-Driven Selective Photocatalytic Hydrogenation of Cinnamaldehyde over Au/SiC Catalysts. *J. Am. Chem. Soc.* **2016**, *138*, 9361-9364.

(10) Hao, C. H.; Guo, X. N.; Sankar, M.; Yang, H.; Ma, B.; Zhang, Y. F.; Tong, X. L.; Jin, G. Q.; Guo, X. Y.: Synergistic Effect of Segregated Pd and Au Nanoparticles on Semiconducting SiC for Efficient Photocatalytic Hydrogenation of Nitroarenes. *ACS Appl. Mater. Interfaces* **2018**, *10*, 23029-23036.

(11) Childs, G. I.; Cooper, A. I.; Nolan, T. F.; Carrott, M. J.; George, M. W.; Poliakoff, M.: A New Approach To Studying the Mechanism of Catalytic Reactions: An Investigation into the Photocatalytic Hydrogenation of Norbornadiene and Dimethylfumarate Using Polyethylene Matrices at Low Temperature and High Pressure. *J. Am. Chem. Soc.* **2001**, *123*, 6857-6866.

(12) Yang, M. Q.; Xu, Y. J.; Lu, W.; Zeng, K.; Zhu, H.; Xu, Q. H.; Ho, G. W.: Self-surface charge exfoliation and electrostatically coordinated 2D hetero-layered hybrids. *Nat. Commun.* **2017**, *8*, 14224.

(13) Yang, M.-Q.; Shen, L.; Lu, Y.; Chee, S. W.; Lu, X.; Chi, X.; Chen, Z.; Xu, Q.-H.; Mirsaidov, U.; Ho, G. W.: Disorder Engineering in Monolayer Nanosheets Enabling Photothermic Catalysis for Full Solar Spectrum (250–2500 nm) Harvesting. *Angew. Chem. Int. Ed.* **2019**, *58*, 3077-3081.

(14) Yang, H. G.; Sun, C. H.; Qiao, S. Z.; Zou, J.; Liu, G.; Smith, S. C.; Cheng, H. M.; Lu, G. Q.: Anatase TiO_2 Single Crystals with a Large Percentage of Reactive Facets. *Nature* **2008**, *453*, 638.

(15) Han, X.; Kuang, Q.; Jin, M.; Xie, Z.; Zheng, L.: Synthesis of Titania Nanosheets with a High Percentage of Exposed (001) Facets and Related Photocatalytic Properties. *J. Am. Chem. Soc.* **2009**, *131*, 3152-3153.

(16) Yang, J.; Wang, D.; Han, H.; Li, C.: Roles of Cocatalysts in Photocatalysis and Photoelectrocatalysis. *Acc. Chem. Res.* **2013**, *46*, 1900-1909.

(17) Weng, B.; Quan, Q.; Xu, Y.-J.: Decorating Geometry- and Size-Controlled Sub-20 nm Pd Nanocubes onto 2D TiO_2 Nanosheets for Simultaneous H_2 Evolution and 1,1-Diethoxyethane Production. *J. Mater. Chem. A* **2016**, *4*, 18366-18377.

(18) Dong, F.; Li, Q.; Sun, Y.; Ho, W.-K.: Noble Metal-Like Behavior of Plasmonic Bi Particles as a Cocatalyst Deposited on (BiO)2CO3 Microspheres for Efficient Visible Light Photocatalysis. *ACS Catal.* **2014**, *4*, 4341-4350.

(19) Li, X.; Bi, W.; Zhang, L.; Tao, S.; Chu, W.; Zhang, Q.; Luo, Y.; Wu, C.; Xie, Y.: Single-Atom Pt as Co-Catalyst for Enhanced Photocatalytic H_2 Evolution. *Adv. Mater.* **2016**, *28*, 2427-31.

(20) Lang, Q.; Yang, Y.; Zhu, Y.; Hu, W.; Jiang, W.; Zhong, S.; Gong, P.; Teng, B.; Zhao, L.; Bai, S.: High-Index Facet Wngineering of PtCu Cocatalysts for Superior Photocatalytic Reduction of CO_2 to CH_4. *J. Mater. Chem. A* **2017**, *5*, 6686-6694.

(21) Chen, Q.; Chen, X.; Fang, M.; Chen, J.; Li, Y.; Xie, Z.; Kuang, Q.; Zheng, L.: Photo-Induced Au–Pd Alloying at TiO_2 {101} Facets Enables Robust CO_2 Photocatalytic Reduction into Hydrocarbon Fuels. *J. Mater. Chem. A* **2019**, *7*, 1334-1340.

(22) Selander, N.; K, J. S.: Catalysis by palladium pincer complexes. *Chem. Rev.* **2011**, *111*, 2048-76.

(23) Negishi, E.-i.; Anastasia, L.: Palladium-Catalyzed Alkynylation. *Chem. Rev.* **2003**, *103*, 1979-2018.

(24) Marshall, J. A.: Synthesis and Reactions of Allylic, Allenic, Vinylic, and Arylmetal Reagents from Halides and Esters via Transient Organopalladium Intermediates. *Chem. Rev.* **2000**, *100*, 3163-

3186.

(25) Li, X.; Zhang, N.; Xu, Y.-J.: Promoting Visible-Light Photocatalysis with Palladium Species as Cocatalyst. *ChemCatChem* **2015**, *7*, 2047-2054.

(26) Zeni, G.; Larock, R. C.: Synthesis of Heterocycles via Palladium π-Olefin and π-Alkyne Chemistry. *Chem. Rev.* **2004**, *104*, 2285-2310.

(27) Adams, B. D.; Chen, A.: The Role of Palladium in a Hydrogen Economy. *Mater. Today* **2011**, *14*, 282-289.

(28) Corvaisier, F.; Schuurman, Y.; Fecant, A.; Thomazeau, C.; Raybaud, P.; Toulhoat, H.; Farrusseng, D.: Periodic Trends in the Selective Hydrogenation of Styrene over Silica Supported Metal Catalysts. *J. Catal.* **2013**, *307*, 352-361.

(29) Xie, S.; Choi, S.-I.; Xia, X.; Xia, Y.: Catalysis on Faceted Noble-Metal Nanocrystals: Both Shape and Size Matter. *Curr. Opin. Chem. Eng.* **2013**, *2*, 142-150.

(30) Shi, Y.; Lyu, Z.; Zhao, M.; Chen, R.; Nguyen, Q. N.; Xia, Y.: Noble-Metal Nanocrystals with Controlled Shapes for Catalytic and Electrocatalytic Applications. *Chem. Rev.* **2020**.

(31) Bai, S.; Wang, X.; Hu, C.; Xie, M.; Jiang, J.; Xiong, Y.: Two-Dimensional g-C_3N_4: An Ideal Platform for Examining Facet Selectivity of Metal Co-Catalysts in Photocatalysis. *Chem. Commun.* **2014**, *50*, 6094-6097.

(32) Cao, S.; Li, Y.; Zhu, B.; Jaroniec, M.; Yu, J.: Facet Effect of Pd Cocatalyst on Photocatalytic CO_2 Reduction over g-C_3N_4. *J. Catal.* **2017**, *349*, 208-217.

(33) Welin, E. R.; Warkentin, A. A.; Conrad, J. C.; MacMillan, D. W.: Enantioselective alpha-Alkylation of Aldehydes by Photoredox Organocatalysis: Rapid Access to Pharmacophore Fragments from beta-Cyanoaldehydes. *Angew. Chem. Int. Ed.* **2015**, *54*, 9668-9672.

(34) Jeong, H. E.; Kim, S.; Seo, M.-g.; Lee, D.-W.; Lee, K.-Y.: Catalytic activity of Pd octahedrons/SiO_2 for the direct synthesis of hydrogen peroxide from hydrogen and oxygen. *J Mol Catal A Chem* **2016**, *420*, 88-95.

(35) Cao, S.; Li, Y.; Zhu, B.; Jaroniec, M.; Yu, J.: Facet effect of Pd cocatalyst on photocatalytic CO_2 reduction over g-C_3N_4. *J Catal* **2017**, *349*, 208-217.

(36) Tian, F.; Zhang, Y.; Zhang, J.; Pan, C.: Raman Spectroscopy: A New Approach to Measure the Percentage of Anatase TiO_2 Exposed (001) Facets. *J. Phys. Chem. C* **2012**, *116*, 7515-7519.

(37) Wu, Z.; Dong, F.; Zhao, W.; Wang, H.; Liu, Y.; Guan, B.: The fabrication and characterization of novel carbon doped TiO_2 nanotubes, nanowires and nanorods with high visible light photocatalytic activity. *Nanotechnology* **2009**, *20*, 235701.

(38) Cong, Y.; Zhang, J.; Chen, F.; Anpo, M.; He, D.: Preparation, Photocatalytic Activity, and Mechanism of Nano-TiO_2 Co-Doped with Nitrogen and Iron (III). *J. Phys. Chem. C* **2007**, *111*, 10618-10623.

(39) Jin, Y.; Li, G.; Zhang, Y.; Zhang, Y.; Zhang, L.: Photoluminescence of anatase TiO_2 thin films achieved by the addition of $ZnFe_2O_4$. *J. Phys. Condens. Matter* **2001**, *13*, 913-918.

(40) Long, R.; Mao, K.; Ye, X.; Yan, W.; Huang, Y.; Wang, J.; Fu, Y.; Wang, X.; Wu, X.; Xie, Y.; Xiong, Y.: Surface facet of palladium nanocrystals: a key parameter to the activation of molecular oxygen for organic catalysis and cancer treatment. *J. Am. Chem. Soc.* **2013**, *135*, 3200-7.

(41) Jiang, B.; Tian, C.; Pan, Q.; Jiang, Z.; Wang, J.-Q.; Yan, W.; Fu, H.: Enhanced Photocatalytic Activity and Electron Transfer Mechanisms of Graphene/TiO_2 with Exposed {001} Facets. *J. Phys. Chem. C* **2011**, *115*, 23718-23725.

(42) Zheng, Z.; Huang, B.; Lu, J.; Qin, X.; Zhang, X.; Dai, Y.: Hierarchical TiO_2 microspheres:

synergetic effect of {001} and {101} facets for enhanced photocatalytic activity. *Chem* **2011**, *17*, 15032-8.

(43) Yang, M.-Q.; Pan, X.; Zhang, N.; Xu, Y.-J.: A facile one-step way to anchor noble metal (Au, Ag, Pd) nanoparticles on a reduced graphene oxide mat with catalytic activity for selective reduction of nitroaromatic compounds. *CrystEngComm* **2013**, *15*, 6819-6828

(44) Hoffmann, M. R.; Martin, S. T.; Choi, W.; Bahnemann, D. W. J. C. r.: Environmental applications of semiconductor photocatalysis. *Chem. Rev.* **1995**, *95*, 69-96.

(45) Sarina, S.; Zhu, H. Y.; Xiao, Q.; Jaatinen, E.; Jia, J.; Huang, Y.; Zheng, Z.; Wu, H.: Viable photocatalysts under solar-spectrum irradiation: nonplasmonic metal nanoparticles. *Angew. Chem. Int. Ed.* **2014**, *53*, 2935-2940.

(46) Jiang, W.; Bai, S.; Wang, L.; Wang, X.; Yang, L.; Li, Y.; Liu, D.; Wang, X.; Li, Z.; Jiang, J.; Xiong, Y.: Integration of Multiple Plasmonic and Co-Catalyst Nanostructures on TiO_2 Nanosheets for Visible-Near-Infrared Photocatalytic Hydrogen Evolution. *Small* **2016**, *12*, 1640-1648.

(47) Weng, B.; Liu, S.; Zhang, N.; Tang, Z.-R.; Xu, Y.-J.: A simple yet efficient visible-light-driven CdS nanowires-carbon nanotube 1D–1D nanocomposite photocatalyst. *J Catal* **2014**, *309*, 146-155.

(48) Kuvarega, A. T.; Krause, R. W. M.; Mamba, B. B.: Nitrogen/Palladium-Codoped TiO_2 for Efficient Visible Light Photocatalytic Dye Degradation. *J. Phys. Chem. C* **2011**, *115*, 22110-22120.

(49) Zhong, J. B.; Lu, Y.; Jiang, W. D.; Meng, Q. M.; He, X. Y.; Li, J. Z.; Chen, Y. Q.: Characterization and photocatalytic property of Pd/TiO2 with the oxidation of gaseous benzene. *J. Hazard. Mater.* **2009**, *168*, 1632-1635.

(50) Shiraishi, Y.; Fujiwara, K.; Sugano, Y.; Ichikawa, S.; Hirai, T.: N-Monoalkylation of Amines with Alcohols by Tandem Photocatalytic and Catalytic Reactions on TiO_2 Loaded with Pd Nanoparticles. *ACS Catal.* **2013**, *3*, 312-320.

(51) Xue, F.; Chen, C.; Fu, W.; Liu, M.; Liu, C.; Guo, P.; Shen, S.: Interfacial and Dimensional Effects of Pd Co-Catalyst for Efficient Photocatalytic Hydrogen Generation. *J. Phys. Chem. C* **2018**, *122*, 25165-25173.

(52) Hulse, J.; Küppers, J.; Wandelt, K.; Ertl, G.: UV-photoelectron Spectroscopy from Xenon Adsorbed on Heterogeneous Metal Surfaces. *Appl. Surf. Sci.* **1980**, *6*, 453-463.

(53) Singh-Miller, N. E.; Marzari, N.: Surface energies, work functions, and surface relaxations of low-index metallic surfaces from first principles. *Phys. Rev. B* **2009**, *80*.

(54) Zhang, N.; Yang, M.-Q.; Tang, Z.-R.; Xu, Y.-J.: Toward Improving the Graphene–Semiconductor Composite Photoactivity via the Addition of Metal Ions as Generic Interfacial Mediator. *ACS Nano* **2014**, *8*, 623-633.

(55) Weng, B.; Wu, J.; Zhang, N.; Xu, Y. J.: Observing the role of graphene in boosting the two-electron reduction of oxygen in graphene-WO_3 nanorod photocatalysts. *Langmuir* **2014**, *30*, 5574-84.

(56) Zhang, N.; Liu, S.; Fu, X.; Xu, Y.-J.: Synthesis of M@TiO_2(M = Au, Pd, Pt) Core–Shell Nanocomposites with Tunable Photoreactivity. *J. Phys. Chem. C* **2011**, *115*, 9136-9145.

(57) Yang, M.-Q.; Weng, B.; Xu, Y.-J.: Synthesis of In_2S_3–CNT nanocomposites for selective reduction under visible light. *J. Mater. Chem. A* **2014**, *2*, 1710-1720.

(58) Pan, X.; Zhao, Y.; Liu, S.; Korzeniewski, C. L.; Wang, S.; Fan, Z.: Comparing graphene-TiO_2 nanowire and graphene-TiO_2 nanoparticle composite photocatalysts. *ACS Appl. Mater. Interfaces* **2012**, *4*, 3944-50.

(59) Weng, B.; Xu, Y.-J.: What if the Electrical Conductivity of Graphene Is Significantly Deteriorated

for the Graphene–Semiconductor Composite-Based Photocatalysis? *ACS Appl. Mater. Interfaces* **2015**, *7*, 27948-27958.

(60) Qiu, B.; Xing, M.; Zhang, J.: Mesoporous TiO_2 nanocrystals grown in situ on graphene aerogels for high photocatalysis and lithium-ion batteries. *J. Am. Chem. Soc.* **2014**, *136*, 5852-5.

(61) Lu, T.; Zhang, Y.; Li, H.; Pan, L.; Li, Y.; Sun, Z.: Electrochemical Behaviors of Graphene–ZnO and Graphene–SnO_2 Composite Films for Supercapacitors. *Electrochim. Acta* **2010**, *55*, 4170-4173.

(62) Weng, B.; Zhang, X.; Zhang, N.; Tang, Z. R.; Xu, Y. J.: Two-dimensional MoS_2 nanosheet-coated Bi_2S_3 discoids: synthesis, formation mechanism, and photocatalytic application. *Langmuir* **2015**, *31*, 4314-22.

(63) Fang, J.; Fan, H.; Li, M.; Long, C.: Nitrogen Self-Doped Graphitic Carbon Nitride as Efficient Visible Light Photocatalyst for Hydrogen Evolution. *J. Mater. Chem. A* **2015**, *3*, 13819-13826.

(64) Cho, C. Y.; Moon, J. H.: Hierarchically porous TiO2 electrodes fabricated by dual templating methods for dye-sensitized solar cells. *Adv. Mater.* **2011**, *23*, 2971-5.

(65) Weng, B.; Zhang, J.; Shi, Z. F.; Tang, Z.; Zheng, L. S.; Xu, Y. J.: Improving the Photostability of Ultrasmall Au Clusters via a Combined Strategy of Surface Engineering and Interfacial Modification. *Langmuir* **2019**, *35*, 5728-5736.

(66) Weng, B.; Lu, K. Q.; Tang, Z.; Chen, H. M.; Xu, Y. J.: Stabilizing ultrasmall Au clusters for enhanced photoredox catalysis. *Nat. Commun.* **2018**, *9*, 1543.

(67) Sing, K. S. J. P.; chemistry, a.: Reporting physisorption data for gas/solid systems with special reference to the determination of surface area and porosity (Recommendations 1984). *Pure Appl. Chem* **1985**, *57*, 603-619.

(68) Wang, Y.; Yang, F. H.; Yang, R. T.; Heinzel, J. M.; Nickens, A. D.: Desulfurization of High-Sulfur Jet Fuel by π-Complexation with Copper and Palladium Halide Sorbents. *Ind. Eng. Chem. Res.* **2006**, *45*, 7649-7655.

(69) Qin, W.; Cao, W.; Liu, H.; Li, Z.; Li, Y.: Metal–organic framework MIL-101 doped with palladium for toluene adsorption and hydrogen storage. *RSC Adv.* **2014**, *4*, 2414-2420.

(70) Klinkova, A.; Cherepanov, P. V.; Ryabinkin, I. G.; Ho, M.; Ashokkumar, M.; Izmaylov, A. F.; Andreeva, D. V.; Kumacheva, E.: Shape-Dependent Interactions of Palladium Nanocrystals with Hydrogen. *Small* **2016**, *12*, 2450-2458.

(71) Li, X.; Wang, C.; Li, B.; Shao, Y.; Li, D.: Efficient light harvesting over a CdS/In_2O_3 photonic crystal photocatalyst for hydrogenation of 4-nitroaniline to p-phenylenediamine. *Phys. Chem. Chem. Phys.* **2016**, *18*, 27848-27857.

(72) Jbarah, A. A.; Holze, R.: A comparative spectroelectrochemical study of the redox electrochemistry of nitroanilines. *J Solid State Electrochem* **2005**, *10*, 360-372.

(73) Fu, Y.; Huang, T.; Zhang, L.; Zhu, J.; Wang, X.: Ag/g-C_3N_4 catalyst with superior catalytic performance for the degradation of dyes: a borohydride-generated superoxide radical approach. *Nanoscale* **2015**, *7*, 13723-33.

Table of Content (TOC)